

Cite this article as: Gao Jianping, Lv Yuanjiang, Li Yongjing, et al. Influence of N₂ Flow Rate on Microstructure and Corrosion Resistance of TaN Coatings on Bipolar Plates of PEM Electrolyser[J]. Rare Metal Materials and Engineering, 2025, 54(05): 1127-1133. DOI: <https://doi.org/10.12442/j.issn.1002-185X.20240720>.

ARTICLE

Influence of N₂ Flow Rate on Microstructure and Corrosion Resistance of TaN Coatings on Bipolar Plates of PEM Electrolyser

Gao Jianping^{1,2}, Lv Yuanjiang¹, Li Yongjing¹, Sun Wenqian¹, Ren Biying², Dai Zhengfei¹, Ma Fei¹

¹ State Key Laboratory for Mechanical Behavior of Materials, Xi'an Jiaotong University, Xi'an 710049, China; ² Western Metal Materials Co., Ltd, Xi'an 710201, China

Abstract: TaN coatings were deposited on Ti bipolar plates by magnetron sputtering to improve corrosion resistance and service life. The influence of N₂ flow rate on the surface morphology, hydrophobicity, crystallinity, corrosion resistance, and interfacial contact resistance of TaN coatings was studied. Results show that as the N₂ flow rate increases, the roughness of TaN coatings decreases firstly and then increases, and the hydrophobicity increases firstly and then decreases. At the N₂ flow rate of 3 mL/min, TaN coating with larger grain size presents lower roughness and high hydrophobicity. The coating possesses the lowest corrosion current density of 2.82 $\mu\text{A}\cdot\text{cm}^{-2}$ and the highest corrosion potential of -0.184 V vs. SCE in the simulated proton exchange membrane water electrolyser environment. After a potentiostatic polarization test for 10 h, a few corrosion pits are observed on the TaN coatings deposited at an N₂ flow rate of 3 mL/min. After 75 h of electrolytic water performance testing, the TaN coating on bipolar plate improves the corrosion resistance and thus enhances the electrolysis efficiency (68.87%), greatly reducing the cost of bipolar plates.

Key words: TaN coatings; corrosion resistance; Ti bipolar plate; water electrolysis

1 Introduction

Proton exchange membrane water electrolyser (PEMWE) is one of the important equipment for solving the issues of environmental pollution^[1-2]. Bipolar plate (BP) as a key component of PEMWE provides structural support for the membrane electrode assembly (MEA), distributes water across the porous transport layer, conducts electrons between cells, and facilitates the mass transport and thermal management. Compared with stainless steel (SS), titanium-based BPs exhibit outstanding corrosion resistance, high electric and thermal conductivity, and excellent mechanical strength^[3]. The Ti BPs used at the anode side typically employ coatings of platinum group metals to achieve better durability and satisfy the performance requirements under high voltage or oxidizing environment conditions. The high corrosion

resistance of titanium favors the chemical stability of the proton exchange membrane (PEM) and catalyst. However, BPs occupy 30% of the PEMWE cell cost and >60% of the mass^[4], and the corrosion is the main failure of BPs^[5-6]. Therefore, anti-corrosion coatings have been explored to enhance the corrosion resistance of BPs and to prolong the service life^[4,7-8]. In addition, the passivation film formed on the metal surface usually results in the elevated interfacial contact resistance (ICR) between BPs and the porous transport layer (PTL)^[9]. The oxide layer formed during electrolysis will also increase ICR values, which leads to a significant decline of electrolysis efficiency and a shortened service life.

Commonly, metallic nitrides with strong ionic bonds exhibit high anti-corrosion properties and are usually applied to protect BPs^[10-14]. For instance, CrN coatings deposited on SS BPs presented high corrosion resistance with a low corrosion

Received date: November 04, 2024

Foundation item: National Key Research and Development Program of China (2022YFB4002100); National Natural Science Foundation of China (52271136); Natural Science Foundation of Shaanxi Province (2021JC-06)

Corresponding author: Ma Fei, Ph. D., Professor, State Key Laboratory for Mechanical Behavior of Materials, Xi'an Jiaotong University, Xi'an 710049, P. R. China, E-mail: mafei@mail.xjtu.edu.cn

Copyright © 2025, Northwest Institute for Nonferrous Metal Research. Published by Science Press. All rights reserved.

current density ($I_{\text{corr}} < 0.26 \mu\text{A}\cdot\text{cm}^{-2}$)^[15-16]. However, C/Al doped-CrN coatings showed degraded corrosion resistance with the higher I_{corr} ($> 0.277 \mu\text{A}\cdot\text{cm}^{-2}$ and even maximum of $0.576 \mu\text{A}\cdot\text{cm}^{-2}$). NbN and TiN coatings on Ti BPs presented excellent corrosion resistance with $I_{\text{corr}} < 0.73 \mu\text{A}\cdot\text{cm}^{-2}$ and low ICR $< 15.8 \text{ m}\Omega\cdot\text{cm}^{2[14,17]}$. TaN ($607 \text{ kJ}\cdot\text{mol}^{-1}$) has a higher bond dissociation energy than TiN ($476 \text{ kJ}\cdot\text{mol}^{-1}$) and NbN ($226 \text{ kJ}\cdot\text{mol}^{-1}$)^[16] and should exhibit better corrosion resistance, but TaN coatings are seldomly focused^[19-20].

In this research, TaN coatings were deposited on Ti BPs via the direct current magnetron sputtering. The influence of N_2 flow rate on the surface morphology, phases, roughness, water contact angle, corrosion resistance, and ICR properties of TaN coatings was studied. The anti-corrosion mechanism was discussed.

2 Experiment

Before coating deposition, pure Ti samples were ground with 800#, 1500#, and 2500# SiC papers, and then ultrasonically cleaned with alcohol and deionized water for 15 min, separately, and finally placed in a low temperature and dust-free environment for natural drying. TaN coatings were deposited on the Ti substrates by reactive sputter-deposition technique (JGP450). The base pressure was 5×10^{-5} Pa. Ar (99.999%) plasma was used to remove the impurities and oxides on the targets and substrate surfaces. Ta target (99.995%, $\Phi = 50$ mm) was used as the metal source with a distance between the target and the substrate of 150 mm, while N_2 gas (99.999% purity) was used as the N source. The N_2 flow rate was 2, 3, 4, and 5 mL/min with the Ar flow rate of 20 mL/min. The work pressure, direct current power, deposition time, and deposition temperature were set as 0.7 Pa, 80 W, 1.5 h, and 150°C , respectively.

X-ray diffraction (XRD, Bruker/D8 Advance, Germany, $\lambda = 0.15405 \text{ nm}$) patterns of TaN coatings were measured at the scanning range of 20° – 80° at an operation voltage of 40 kV and an operation current of 30 mA. The surface and cross-section morphologies were characterized by field emission scanning electron microscope (JSM-7001F, JEOL Ltd, Tokyo, Japan) equipped with energy dispersive spectroscopy (EDS) at an operation voltage of 15 kV and an operation current of 25 pA. The roughness was tested by confocal laser scanning microscope (Olympus, OLS5100). The surface wettability of the coatings was investigated by measuring the static contact angle (θ) at the ambient temperature, atmospheric pressure, and relative humidity of 45%. The contact angle was measured using a 2 mL water droplet by a contact angle measuring apparatus.

Potentiodynamic polarization was performed in an electrochemical cell consisting of a three-electrode test system using a platinum sheet as counter electrode and a saturated calomel electrode (SCE) connected to a Luggin capillary filled with saturated KCl solution as reference electrode. TaN coatings on Ti were served as the working electrode. The potentiodynamic and potentiostatic polarization tests of TaN coatings were conducted in PEMWE simulated acidic aqueous

environment ($0.5 \text{ mol/L H}_2\text{SO}_4 + 2 \times 10^{-4} \text{ wt\% F}^-$) at 80°C via the electrochemical workstation (Autolab-PGSTAT 128 N). The potentiodynamic polarization test was conducted from -1.0 V vs. RHE to 2.5 V vs. RHE at a scanning rate of $1 \text{ mV}\cdot\text{S}^{-1}$ after the open-circuit potential (OCP) for 1 h. The potentiostatic polarization was operated at 2 V.

ICR between the sample surface and PTL was determined by PEM fuel cell test method. The sample was placed between two pieces of conductive carbon paper (Toray TGP-H-090) and then sandwiched between two Au-coated copper plates. The applied current was stabilized at 1.5 A with the compaction force on the two Au-coated copper plates increasing gradually from 0.1 MPa to 2.0 MPa. The corresponding voltage was recorded to calculate the total resistance as a function of compaction force. The resistance of the carbon paper was measured in the same way and subsequently subtracted from the total resistance^[12]. ICR values were obtained at a conventional compaction pressure of 1.5 MPa.

PEM electrolyser cell consisting of multi-channel flow field Ti BPs was manufactured with an active surface area of $70 \text{ mm} \times 120 \text{ mm}$. The TaN coating was deposited on anode BPs by magnetron sputtering. The sintered Ti fiber felt coated with Pt (500 nm) by electroplating was used as PTL of anode and cathode. A commercially available MEA was used, which consisted of a Nafion 115 membrane, Ir-based anode catalyst, and Pt-based cathode catalyst. The catalyst loading was 1.0 and $0.5 \text{ mg}\cdot\text{cm}^{-2}$. A testing station for PEM electrolyser measurements was assembled, including programmable power supply module, gas-water separators, computer control module, and thermostatic circulating water module. Ultrapure water (conductivity $< 5 \mu\text{S}\cdot\text{cm}^{-1}$) was used, and it was heated up to 80°C and supplied to the anode side by a peristaltic pump at a flow rate of $400 \text{ mL}\cdot\text{min}^{-1}$.

3 Results and Discussion

3.1 XRD patterns of TaN coatings prepared at different N_2 flow rates

Fig. 1 shows XRD patterns of TaN coatings prepared at different N_2 flow rates. As the N_2 flow rate increases from 2 mL/min to 4 mL/min, the crystallinity of TaN coating is

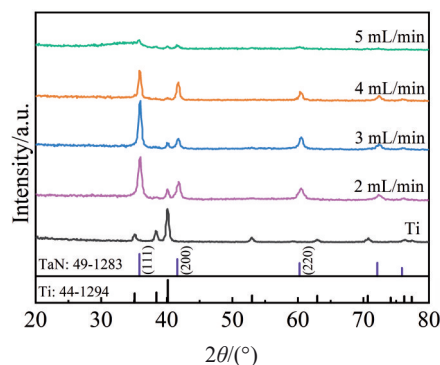


Fig.1 XRD patterns of TaN coatings prepared at different N_2 flow rates

improved with the preferred TaN (111) orientation. XRD peaks at $2\theta=35.83^\circ$, 41.46° , 60.26° , and 72.12° correspond to (111), (200), (220), and (311) planes of cubic TaN phase. However, as the N_2 flow rate further increases to 5 mL/min, the crystallinity of TaN coatings decreases and even becomes amorphous. The N atomic content increases with the gradual increase in N_2 flow rate, and reaches 55.64at% at N_2 flow rate of 5 mL/min. EDS results of element content of TaN coatings prepared at different N_2 flow rates are shown in Table 1^[14,21]. For reactive sputtering, as the nitrogen flow rate increases, the collision probability between sputtered Ta atoms and the plasma will be increased, thus the sputtered Ta atoms carry less kinetic energy, and the bombardment of Ta and N atoms on Ti substrates as well as on the coatings is weaker. This phenomenon leads to slower nucleation of the coating and smaller nuclei. Particularly, when the stoichiometric ratio of N to Ta exceeds 1:1 (N percentage is 55.64at%, as listed in Table 1), the atoms with lower kinetic energy pile up into an amorphous structure.

3.2 Surface roughness and hydrophobicity of TaN coatings

Fig.2a₁–2d₁ show the surface morphologies of TaN coatings observed by confocal laser scanning microscope. All coatings exhibit smooth morphology with color changing from brown

Table 1 EDS results of element content of TaN coatings prepared at different N_2 flow rates^[14,21]

N_2 flow rate/mL·min ⁻¹	Ta/at%	N/at%
2	47.78	52.22
3	46.89	53.11
4	46.58	53.42
5	44.36	55.64

to gray, which can be ascribed to different surface roughness and crystal structures^[22]. Fig. 2a₂–2d₂ show the grayscale images of surface roughness. The average arithmetic roughness (S_a) of TaN coatings prepared at N_2 flow rate of 2, 3, 4, and 5 mL/min is 0.054, 0.036, 0.052, and 0.052 μm , respectively. The TaN coating prepared at N_2 flow rate of 3 mL/min has the smallest surface roughness with less pits and gullies, which can prolong the service life of BPs^[14,23]. As illustrated in Fig. 2a₃–2d₃, the water contact angles of TaN coatings are all above 90° , indicating hydrophobicity, and the TaN coating prepared at N_2 flow rate of 3 mL/min presents the lowest hydrophobicity.

3.3 Surface morphology of TaN coatings

Fig.3 shows the cross-section and surface morphologies of

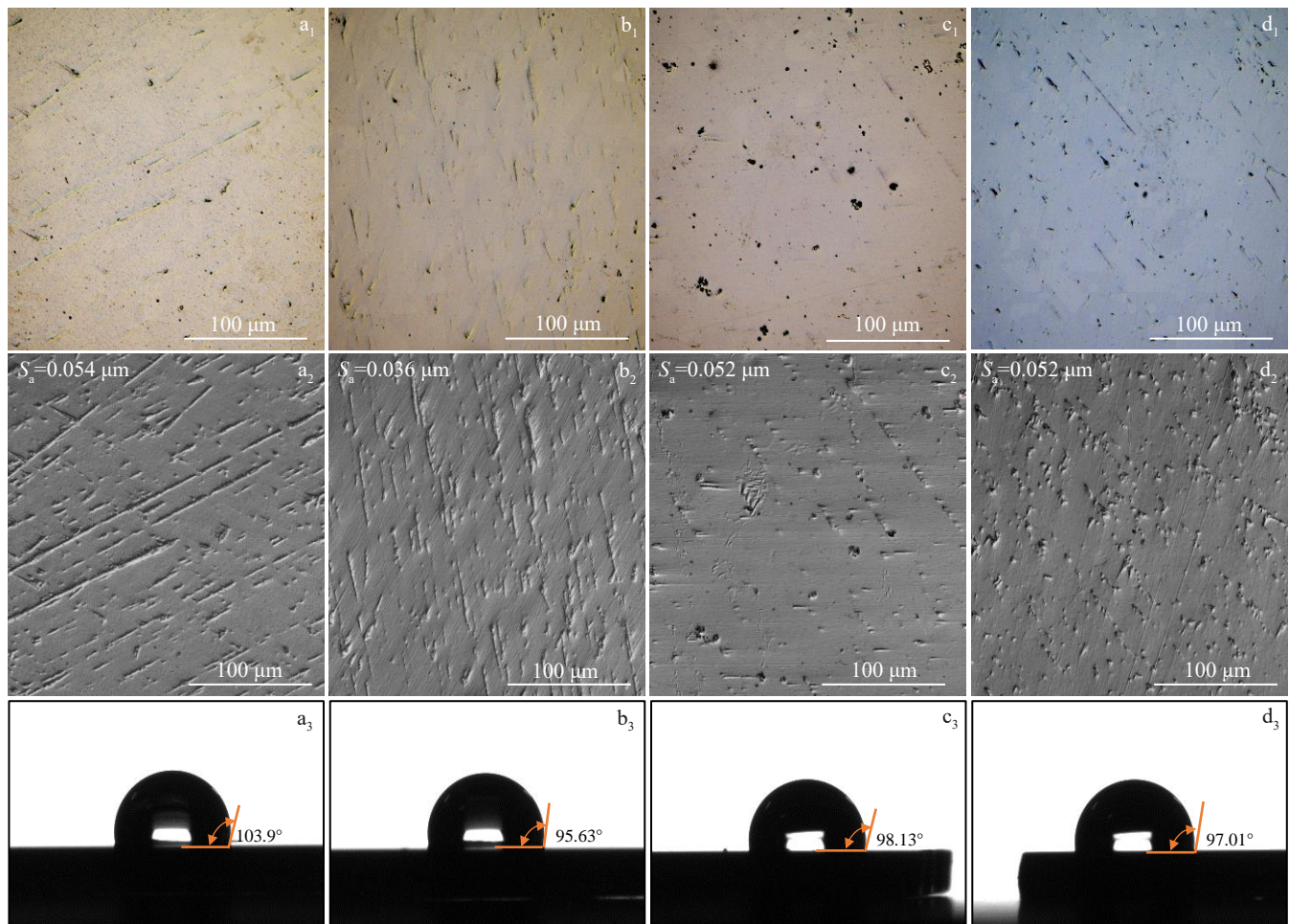


Fig.2 Surface morphologies (a₁–d₁), surface roughness (a₂–d₂), and water contact angles (a₃–d₃) of TaN coatings prepared at N_2 flow rate of 2 mL/min (a₁–a₃), 3 mL/min (b₁–b₃), 4 mL/min (c₁–c₃), and 5 mL/min (d₁–d₃)

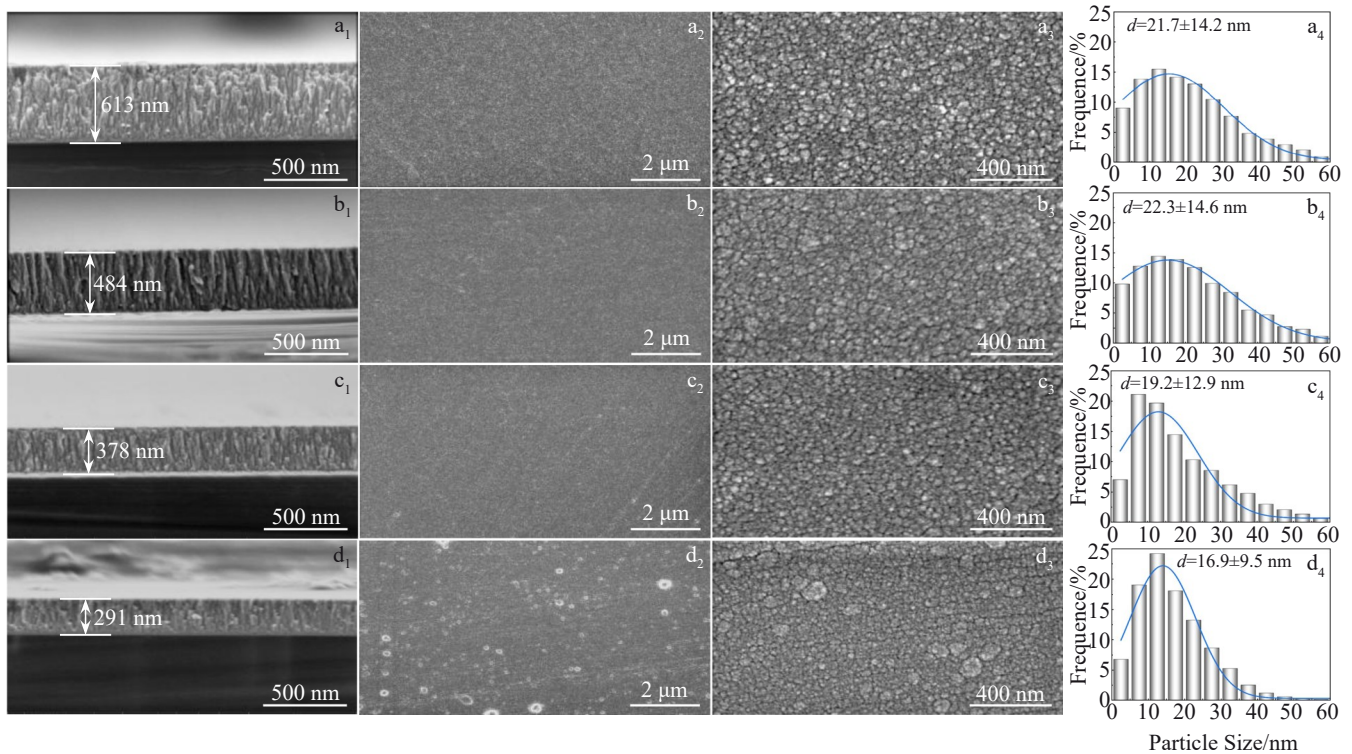


Fig.3 Cross-section morphologies (a₁–d₁), surface morphologies (a₂–d₂, a₃–d₃), and grain size distributions (a₄–d₄) of TaN coatings prepared at N₂ flow rate of 2 mL/min (a₁–a₄), 3 mL/min (b₁–b₄), 4 mL/min (c₁–c₄), and 5 mL/min (d₁–d₄)

different TaN coatings. As displayed in Fig. 3a₁–3d₁, the coatings are composed of columnar-like grains, and the thickness decreases with the increase in N₂ flow rate. Since the ionization energy of N is higher than that of Ar, the plasma is reduced with the increase in N₂ flow rate, and thus the deposition of TaN slows down. Fig. 3a₂–3d₂ and 3a₃–3d₃ show the surface morphologies of different TaN coatings. Fig. 3a₄–3d₄ present the grain size distributions of different TaN coatings. For the coatings deposited at N₂ flow rate of 2 and 3 mL/min, the surface morphologies are smooth with larger grain sizes. However, if the N₂ flow rate further increases to 4 and 5 mL/min, the surface morphologies become rougher with some ridges and particles (Fig. 3c₂ and 3d₂). Meanwhile, the average grain size decreases (Fig. 3c₄ and 3d₄).

3.4 Corrosion resistance of TaN coatings

The cathodic Tafel slope (β_c) and anodic Tafel slope (β_a) are obtained through linear fitting of the cathode and anodic Tafel regions of the corrosion polarization curves. The intersection of cathode Tafel fitting curve and anode Tafel fitting curve is self-corrosion current density (I_{corr}) and corrosion potential (E_{corr}), respectively. The polarization resistance (R_p) can be calculated by Eq.(1)^[24], as follows:

$$R_p = \frac{\beta_a \beta_c}{2.303 \times I_{corr} (\beta_a + \beta_c)} \quad (1)$$

where β_c is the cathodic Tafel slope and β_a is the anodic Tafel slope.

Fig. 4a–4b show the polarization curves of different TaN coatings. The current density@2V indicates the current density value at 2 V; the ICR@1.5MPa indicates ICR value at

compression force of 1.5 MPa. The self-corrosion current density (I_{corr}), corrosion potential (E_{corr}), cathodic Tafel slope (β_c), anodic Tafel slope (β_a), polarization resistance (R_p), and corrosion current density at 2 V (I_{2V}) are summarized in Table 2. For the TaN coating prepared at N₂ flow rate of 3 mL/min, the corrosion resistance of the coating is improved with lower I_{corr} of 2.82 $\mu\text{A}\cdot\text{cm}^{-2}$ and higher E_{corr} of -0.184 V vs. SCE, because of the lower roughness (Fig. 2b₂) and high hydrophobicity (Fig. 2b₃). If the N₂ flow rate further increases to 5 mL/min, the corrosion resistance of TaN coating decreases with higher I_{corr} of 110.70 $\mu\text{A}\cdot\text{cm}^{-2}$ and the lower E_{corr} of -0.434 V vs. SCE, which results from the increased roughness and more surface defects. Because PEMWE generally works at a higher voltage (>1.6 V)^[14], the corrosion current density at 2 V (I_{2V}) is also measured, and the results are displayed in Fig. 4b. The TaN coating prepared at N₂ flow rate of 3 mL/min also exhibits the lowest I_{2V} of 28.5 $\mu\text{A}\cdot\text{cm}^{-2}$, but the the corrosion current density at 2 V is 10 times larger than the self-corrosion current density because of the accelerated corrosion at the higher operating voltage of 2 V. Fig. 4c and 4d show ICR values of different TaN coatings. ICR values decrease with the increase in compaction force. ICR@1.5MPa value increases with the increase in N₂ flow rate. The ICR@1.5MPa values are 11.48, 21.13, 70.28, and 3227.00 $\text{m}\Omega\cdot\text{cm}^2$ when the N₂ flow rate is 2, 3, 4, and 5 mL/min, respectively. ICR@1.5MPa value of the TaN coating prepared at N₂ flow rate of 5 mL/min increases by two orders of magnitude, which may be due to the amorphous feature.

Fig. 5 shows surface morphologies of Ti BP and different TaN coatings after potentiostatic tests in simulated PEMWE

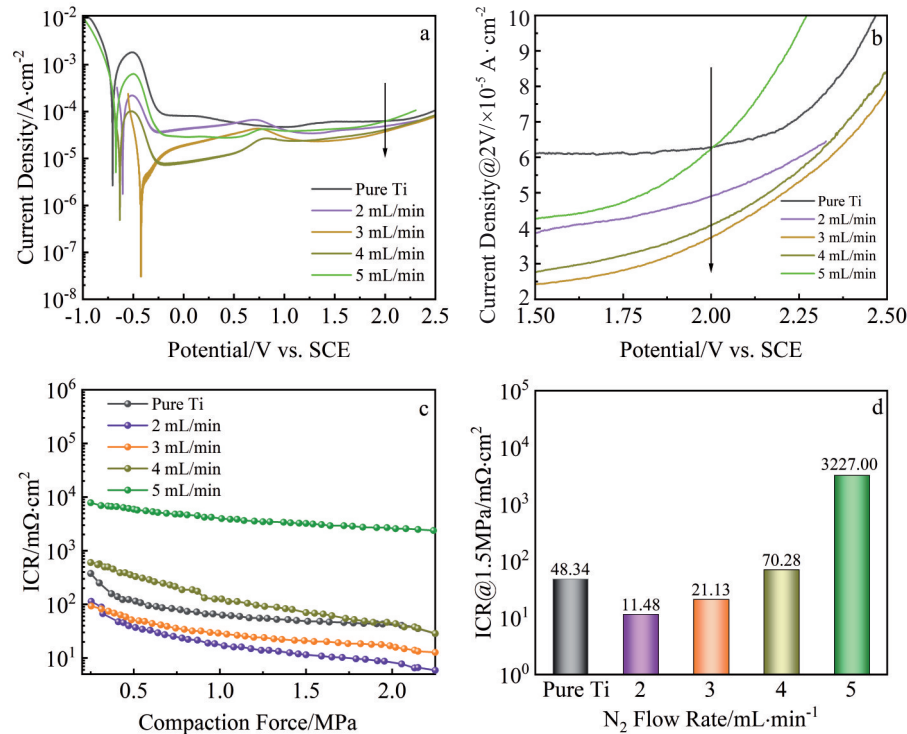


Fig.4 Polarization curves of pure Ti BP and TaN coatings deposited at different N_2 flow rates (a–b); ICR of pure Ti BP and different TaN coatings as a function of compaction force (c); ICR of pure Ti BP and different TaN coatings at compaction force of 1.5 MPa (d)

Table 2 Corrosion properties of pure Ti BP and TaN coatings prepared at different N_2 flow rates

N_2 flow rate/ $\text{mL} \cdot \text{min}^{-1}$	$E_{\text{corr}}/\text{V vs. SCE}$	$I_{\text{corr}}/\mu\text{A} \cdot \text{cm}^{-2}$	$I_{2V}/\mu\text{A} \cdot \text{cm}^{-2}$	$\beta_c/\text{mV} \cdot \text{dec}^{-1}$	$\beta_a/\text{mV} \cdot \text{dec}^{-1}$	$R_p/\Omega \cdot \text{cm}^2$	$r_{\text{corr}}/\text{mm} \cdot \text{a}^{-1}$
Pure Ti BP	-0.463	313.5	61.1	-81.6	135.6	125	3.640
2	-0.363	86.68	42.9	-75.9	202.5	570	1.010
3	-0.184	2.82	28.5	-65.9	308.5	15 758	0.033
4	-0.391	23.23	32.6	-51.5	136.6	1262	0.270
5	-0.434	110.70	60.04	-86.3	120.7	433	1.290

Note: I_{2V} is denoted as the corrosion current density at 2 V

acidic aqueous environment ($0.5 \text{ mol/L H}_2\text{SO}_4 + 2 \times 10^{-4} \text{ wt\% F}^-$) at 2 V and 80°C for 10 h. As displayed in Fig.5a, the surface of pure Ti BP is destroyed with obvious titanium grain boundaries after acid corrosion. However, the surface morphology of Ti BP coated with TaN is well maintained after potentiostatic polarization at 2 V for 10 h. The corrosion pits increase firstly and then decrease. Particularly, for the TaN coating deposited at N_2 flow rate of 3 mL/min, less corrosion pits can be observed due to the higher corrosion resistance. For the TaN coatings prepared at N_2 flow rate of 4 and 5 mL/min, more defects emerge after potentiostatic polarization test for 10 h (Fig.5d and 5e).

3.5 PEM electrolyser test of TaN coated Ti BP

Taking the TaN coating deposited at N_2 flow rate of 3 mL/min as an example, the coated anode and cathode Ti BPs with an active surface area of 80 cm^2 were tested in PEM electrolyser. Fig.6a shows the polarization curves measured at 80°C . The potential of the cell assembled with pure Ti BP is 2.472 V at the current density of $2 \text{ A} \cdot \text{cm}^{-2}$. Compared with that of pure Ti BP, the electrolytic potential of TaN coated Ti

BP is reduced by 323 mV at the current density of $2 \text{ A} \cdot \text{cm}^{-2}$, implying the improved electric conductivity. As a contrast, TiN coatings on Ti sheet^[25] and Pt/Ti coatings on SS^[26] demonstrate the electrolytic potential of about 2.35 V at $1.5 \text{ A} \cdot \text{cm}^{-2}$ and 2.25 V at $2 \text{ A} \cdot \text{cm}^{-2}$, respectively. So the corrosion resistance and electrical conductivity of TaN coatings are higher than those of TiN coatings and Pt/Ti coatings. Compared with the thermoneutral voltage ($V_{\text{tn}} = 1.48 \text{ V}$) in the polarization curves, the electrolysis efficiency is determined^[27]. At the current density of $1 \text{ A} \cdot \text{cm}^{-2}$, the electrolysis efficiency of the electrolyser increases from 59.87% (pure Ti BP) to 68.87% (TaN coated Ti BPs), owing to the reduced ICR between Ti BP and PTL. Then, the electrolytic cell was tested at a constant current density of $2 \text{ A} \cdot \text{cm}^{-2}$ for 75 h. The electrolytic potential of the pure Ti BP rapidly increases above 2.6 V after 35 h, demonstrating the failure of the pure Ti BP. However, the electrolytic voltage of TaN coated Ti BPs is increased slightly from 1.968 V to 2.02 V after test for 75 h. Comparatively, the electrolytic potential of TiN coatings is slightly increased from 2.35 V to

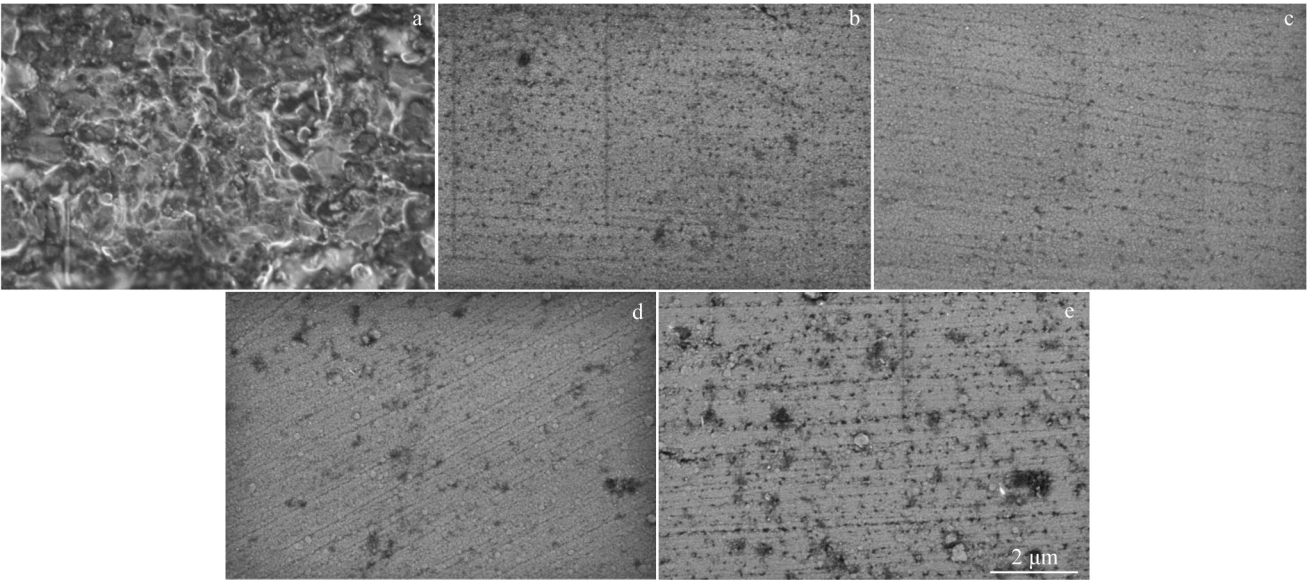


Fig.5 Surface morphologies of pure Ti BP (a) and TaN coatings prepared at different N_2 flow rates (b–d) after potentiostatic polarization test for 10 h: (b) 2 mL/min, (c) 3 mL/min, (d) 4 mL/min, and (e) 5 mL/min

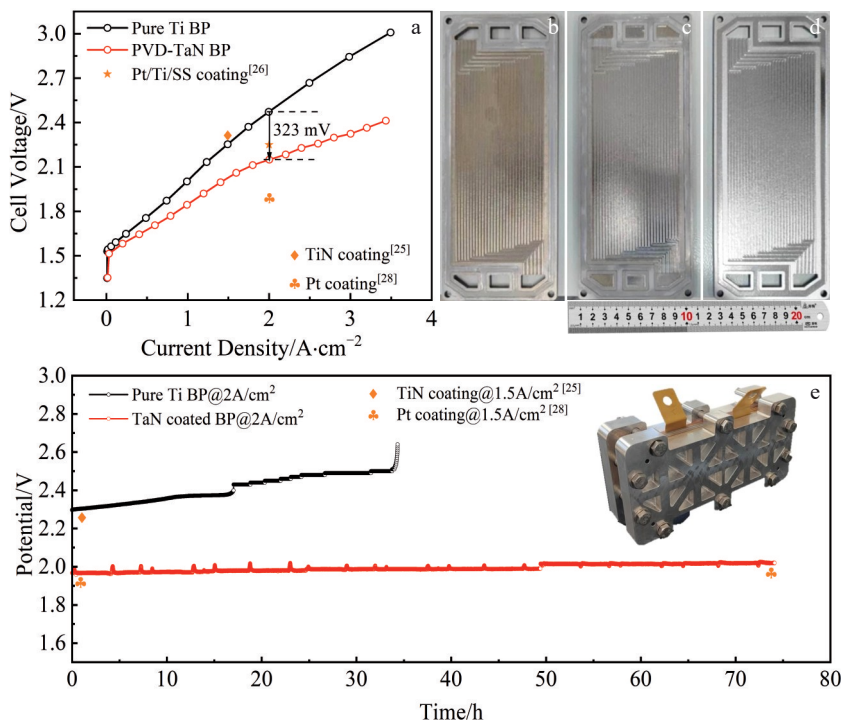


Fig.6 Polarization curves of electrolyser assembled with Ti BPs without and with TaN coatings (a); appearance of different Ti BPs after water electrolysis: (b) pure Ti plate, (c) anodic TaN coated Ti BP, and (d) cathodic TaN coated Ti BP; cell voltage of Ti BPs in single electrolysis cell at $2\text{ A}\cdot\text{cm}^{-2}$ (e)

2.37 V under $1.5\text{ A}\cdot\text{cm}^{-2}$ after 100 h^[25], and that of Pt coatings is only increased from 1.870 V to 1.875 V under $1.5\text{ A}\cdot\text{cm}^{-2}$ after 96 h^[28]. So the stability of TaN coatings is comparable to that of Pt coatings. This result indicates that TaN coatings with low cost exhibit a great engineering significance for reducing the cost of BPs. The fluctuations can be ascribed to the temperature fluctuations of circulating water in the electrolytic cell. As shown in Fig. 6b–6d, Ti BPs are oxidized and turn yellow after electrolysis test. At the same time, TaN coatings

on the anode BPs become soft gray as a result of corrosion under saturated O_2 condition and at higher operating potential.

4 Conclusions

1) As N_2 flow rate increases, the surface roughness of TaN coatings decreases firstly and then increases, and correspondingly the hydrophobicity of coatings increases firstly and then decreases. TaN coating prepared at N_2 flow rate of

3 mL/min presents lower surface roughness and better hydrophobicity.

2) The TaN coating deposited at N_2 flow rate of 5 mL/min becomes amorphous with many particles on the surface. Consequently, TaN coatings prepared at N_2 flow rate of 3 mL/min exhibit the optimal corrosion resistance with the lowest I_{corr} of $2.82 \mu\text{A}\cdot\text{cm}^{-2}$ and the highest E_{corr} of -0.184 V vs. SCE.

3) TaN coating prepared at N_2 flow rate of 5 mL/min exhibits degraded corrosion resistance, and many corrosion pits emerge on the surface after potentiostatic polarization test for 10 h. The electrolysis efficiency of the electrolyser is increased from 59.87% (pure Ti BP) to 68.87% (TaN coated Ti BP) at the current density of $1 \text{ A}\cdot\text{cm}^{-2}$.

4) Moreover, the TaN coated Ti BPs exhibit better stability after water electrolysis at a constant current density of $2 \text{ A}\cdot\text{cm}^{-2}$ for 75 h, which is comparable to that of Pt coatings. This result indicates that TaN coatings with low cost exhibit a great engineering significance for reducing the cost of BPs.

References

- Tao L, You K T, Yan L W et al. *Fuel*[J], 2024, 368: 131610
- Ibuki S, Koichiro F, Mikito U et al. *Fusion Engineering and Design*[J], 2024, 202: 114420
- Yang G, Yu S, Kang Z et al. *Energy Conversion and Management*[J], 2019, 182: 108
- Yuan J L, Jian P G, Qiao M L et al. *The Journal of Physical Chemistry C*[J], 2024, 128: 8123
- Li W K, Xie Z Y, Zeng H D. *RSC Advances*[J], 2024, 14: 7172
- Cui Y F, Cui J L, Xu X et al. *Fuel Cells*[J], 2017, 17: 698
- Peng F Y, Tao Y, Yao Y et al. *Corrosion Science*[J], 2022, 197: 110086
- Deng Z Z, Dai Z F, Wu W B et al. *Rare Metal Materials and Engineering*[J], 2024, 53(10): 2755
- Fang Y Y, Bai I J, Zi Y W et al. *Materials Chemistry and Physics*[J], 2022, 287: 126082
- Jun Y C, Sam Z, Jia Z et al. *Journal of Alloys and Compounds*[J], 2024, 976: 173300
- Mo H C, Ji C D, Se H K et al. *Corrosion Science*[J], 2022, 196: 110042
- Wen Q S, Yuan J L, Jian P G et al. *Journal of Materials Science & Technology*[J], 2025, 210: 86
- Hai T Z, Dong L G, Hong Z D et al. *Surface and Coatings Technology*[J], 2024, 483: 130769
- Fei F B, Pei Y Y, Tao Z et al. *International Journal of Hydrogen Energy*[J], 2015, 40: 9790
- Gao Y L, Dong F S, Bai Z F et al. *International Journal of Hydrogen Energy*[J], 2023, 48: 18996
- Haynes W M, David R L, Thomas J B et al. *CRC Handbook of Chemistry and Physics*[M]. Boca Raton: CRC Press, 2016
- Chang H C, Hyoseok C, Wonhyuk H et al. *International Journal of Hydrogen Energy*[J], 2012, 37: 405
- Lucia M, Anders O, Ole E K et al. *International Journal of Hydrogen Energy*[J], 2017, 42: 3259
- Manaud J P, Poulon A, Gomez S et al. *Surface and Coatings Technology*[J], 2007, 202: 222
- Jian M W, Ji Y Z. *Journal of Alloys and Compounds*[J], 2024, 976: 173300
- Hock C L, Bee H L, Mohd S M et al. *International Journal of Hydrogen Energy*[J], 2024, 57: 420
- Donald H, Hadi A, Andrew R B et al. *Journal of Colloid and Interface Science*[J], 2019, 543: 328
- Gago A S, Ansar S A, Saruhan B et al. *Journal of Power Sources*[J], 2016, 307: 815
- Amin M A, Khaled K F, Fadl-Allah S A. *Corrosion Science*[J], 2010, 52: 140
- Toops T J, Brady M P, Zhang F Y et al. *Journal of Power Sources*[J], 2014, 272: 954
- Gago A S, Ansar S A, Saruhan B et al. *Journal of Power Sources*[J], 2016, 307: 815
- Jason K L, Tobias S, Guido B et al. *Applied Energy*[J], 2023, 33: 120853
- Wang X F, Luo H, Cheng H X et al. *Applied Energy*[J], 2023, 357: 122517

氮气流量对质子交换膜电解槽双极板上 TaN 涂层微观结构与耐腐蚀性能的影响

高建平^{1,2}, 吕源江¹, 李永婧¹, 孙雯倩¹, 任碧莹², 戴正飞¹, 马飞¹

(1. 西安交通大学 金属材料强度国家重点实验室, 陕西 西安 710049)

(2. 西部金属材料股份有限公司, 陕西 西安 710201)

摘要: 通过磁控溅射在钛基双极板上沉积了 TaN 涂层, 以提高其耐腐蚀性和使用寿命, 并研究了氮气流量对 TaN 涂层的表面形貌、疏水性、结晶度、耐腐蚀性能和界面接触电阻的影响。结果表明: 随着氮气流量的增加, TaN 涂层的粗糙度先减小后增大, 疏水性先增大后减小。在氮气流量为 3 mL/min 时, TaN 涂层晶粒较大, 呈现出较低的粗糙度和较高的疏水性。在模拟的质子交换膜电解槽环境中, 该涂层具有最低的腐蚀电流密度 ($2.82 \mu\text{A}\cdot\text{cm}^{-2}$) 和最高的自腐蚀电位 (-0.184 V vs. SCE)。经过 10 h 恒电位极化测试后, 在氮气流量为 3 mL/min 时沉积的 TaN 涂层上观察到的腐蚀坑较少。经过 75 h 的电解水性能测试, TaN 涂层提高了钛双极板腐蚀电阻, 进而提高了电解池的电解效率 (68.87%), 大幅度降低双极板成本。

关键词: TaN 涂层; 耐腐蚀性能; 钛双极板; 水电解

作者简介: 高建平, 男, 1991 年生, 博士生, 西安交通大学金属材料强度国家重点实验室, 陕西 西安 710049, E-mail: gjp_nwpu@163.com